Computer Prediction of the Deformed Shape of a Draw Blank During the Binder-Wrap Stage

SING C. TANG

A method has been developed for predicting the draw-cavity shape of a draw blank during the blank-holder closed, predraw punch impact stage in the sheet metal draw stamping process. By selecting and progressively feeding particular increments of a proposed set of blank holder surface displacements as input boundary conditions, the nonlinear shell computer program developed by Ford Research is utilized to accurately predict the deformed shape of a blank during this stage. The method and computer program have been successfully applied to several symmetrical body panels on an experimental basis. Further work is required to both expand the scope and provide a practical system for the production engineering of sheet metal stampings. However, this method represents a step forward to computerized predictive binder design.

INTRODUCTION

In order to predict which points on a blank contact a punch first as it moves in the sheet metal stamping process, we must know the deformed shape of the blank during the binder-wrap stage. A simplified draw blank to form a car body panel is shown in Fig. 1 and its edges are deformed to the shape of a binder, as shown in Fig. 2. In this blank, we assume two sides are free of force before the punch contacts the blank. The conventional computer graphics method of finding the deformed shape of a blank is by means of fitting the deformed surface with conical, cylindrical, and flat surfaces. This method could predict a deformed center section of the blank, as shown by the dotted line in Fig. 2. It gives excellent agreement with that actually measured from the trial blank in the plaster shop for regions close to two sides over the punch opening; however, this prediction deviates much from that actually measured, as shown by dots in the same figure. As a matter of fact, the middle portion of this center section deforms differently from that at the binder edge such that this portion is a surface with double curvature, and it cannot be treated by the conventional method of fitting a cylindrical surface in that portion. The deformed surface with double curvature cannot be fitted by a set of developable surfaces. Because of the special characteristic of the deformation, the punch might contact there first; therefore, an accurate prediction of the deformed shape, especially in the middle portion, is necessary to determine the initial punch contact.

Invoking the theory of elasticity or plasticity, this is a boundary value problem, with either displacements or forces specified at the blank holder surface which defines the deformed shape of a supported blank before punch contact. We note that the displacement of a point from the undeformed to the deformed state, for exam-

SING C. TANG, Engineering & Research Staff, Research, Ford Motor Company, Dearborn, MI 48121.

ISSN 0162-9700/80/0706-0022$00.75/0

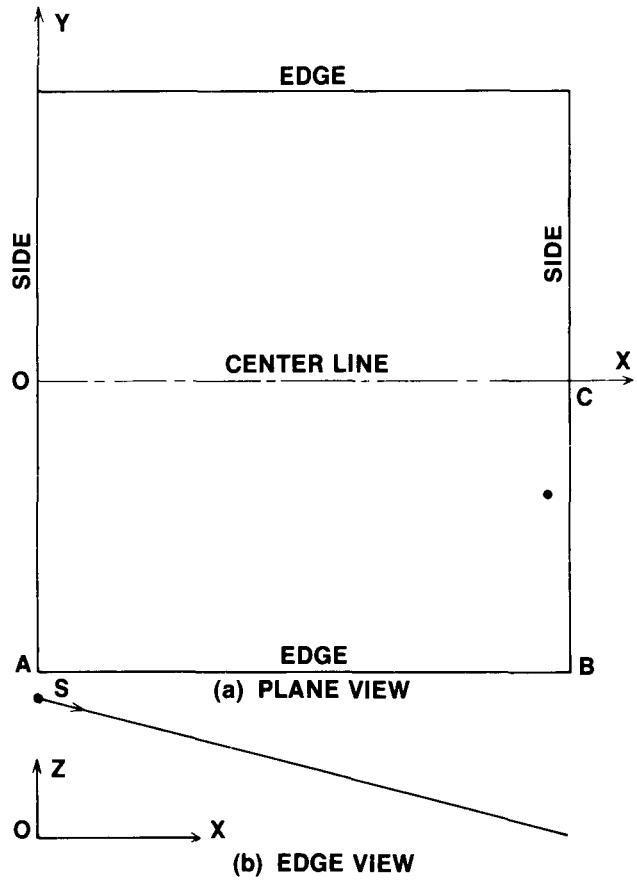

Fig. 1—A simplified rectangular draw blank.

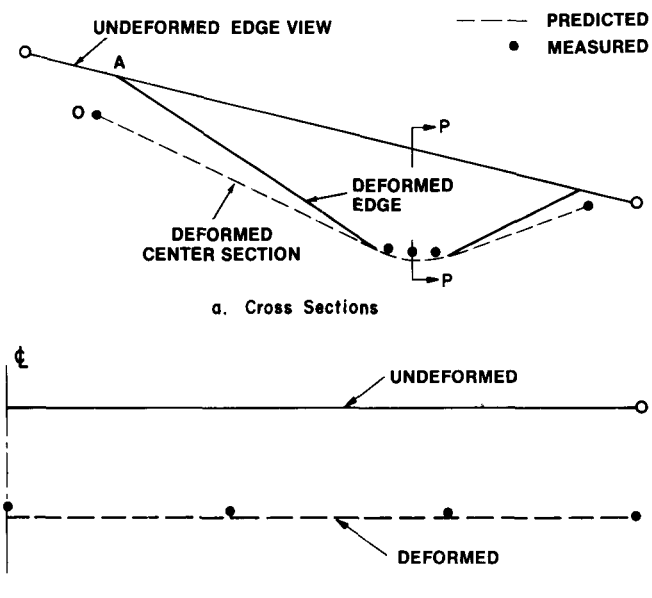

Fig. 2—Deformed edge and center section of simple draw blank during the binder-wrap stage.

ple a point located at the center of the edge, is very large and has the order of magnitude of the blank length or width. The classic linear theory will not be valid to compute deflection of that order of magnitude and we must apply the theory including the geometrical nonlinearity due to large deflection. This complicates solution procedures. Fortunately, the present technique utilizing the finite element method is feasible for solving those nonlinear structure problems, resulting in the prediction of stresses and deformations.

THE FINITE ELEMENT METHOD APPLIED TO NONLINEAR ANALYSIS

We will briefly discuss the finite element method for stress and deformation analysis in this paper. For a complete understanding of this method, an analyst must have a reasonable background of elasticity, matrix algebra, and numerical analysis. There were a series of articles[1] which introduced the finite element method for those who are only familiar with elementary strength of materials. We shall summarize those articles in the appendix.

The formulation in the appendix is valid only if the deformed configuration is not much different from the original shape and the stress is small enough so that the linear relationship (proportionality) between the stress and strain holds. This is the linear theory which most people are using in structural design. If any of the previously mentioned conditions is violated, the nonlinear theory must be used for a correct solution. Figure 3 shows a slender arch under a concentrated load P. When P is small, the deformed configuration (the dotted line in the figure) is not much different from the original (the solid line); therefore, we may use the original shape as the reference configuration to establish the equilibrium conditions without introducing much error. When P is large, the deformed configuration could change from the convex to the concave (the chain line in Fig. 3) and the axial force N changes from compression to tension. The deformed configuration must be used as the reference to establish the equilibrium condition. This is the geometrical nonlin-

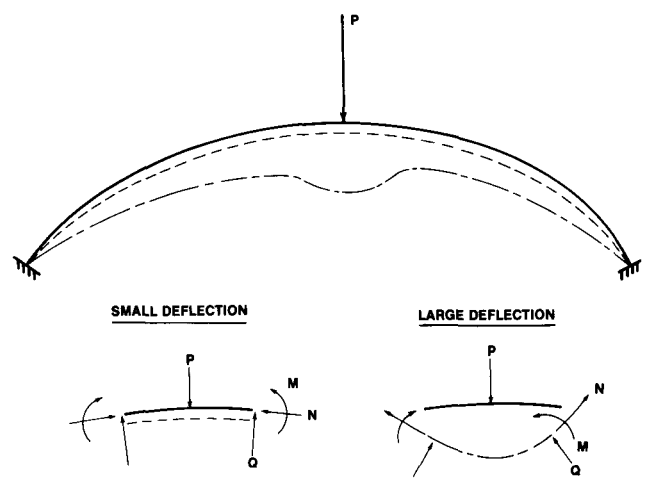

Fig. 3—Deformed configuration of a slender arch under a concentrated load.

earity due to large deflection. In consideration of the geometrical nonlinearity, the stiffness matrix K in Eq. [A8] is no longer constant and it depends upon the solution; therefore, the equilibrium conditions are expressed by a set of nonlinear simultaneous algebraic equations.

The material nonlinearity also exists for most metals, if the stress at a point exceeds a certain level known as the yield strength of the material, there is plastic flow (permanent deformation after the load is completely released and the stress-strain relationship is no longer linear, as shown in Fig. 4. This is known as material nonlinearity. If there is plastic flow, the stress-strain relationship in Eq. [A2] is not valid. Based upon the Prandtl-Reuss relation,[2] Eq. [A2] is changed to the incremental form, as follows:

$$\mathbf{d}\underset{\sim}{\sigma} = \underset{\approx}{D}\mathbf{d}\underset{\sim}{\epsilon} \qquad [1]$$

in which $\mathbf{d}\underset{\sim}{\sigma}$ is the stress incremental vector, $\mathbf{d}\underset{\sim}{\epsilon}$ the strain incremental vector, and $\underset{\approx}{D}$ the material matrix which depends upon the stress level at a point in each element.

Consequently, Eq. [A8] is changed to

$$\underset{\approx}{K}\mathbf{d}\underset{\sim}{\delta} = \mathbf{d}\underset{\sim}{F} \qquad [2]$$

in which $\mathbf{d}\underset{\sim}{\delta}$ and $\mathbf{d}\underset{\sim}{F}$ are increments of the displacement and load vectors, respectively. A step-by-step numerical integration technique can be applied to find the displacement vector $\underset{\sim}{\delta}$ at the load vector $\underset{\sim}{F}$. For a linear problem where K is constant, we need only a one-step solution to obtain $\underset{\sim}{\delta}$.

METHOD OF SOLUTION

Because the thickness of a blank in sheet metal stamping process is small in comparison to its sides or the radius of curvature of a binder section, the nonlinear thin shell theory can be applied instead of the real three-dimensional theory of elasticity or plasticity. This reduces the number of degrees of freedom by one order of magnitude. In thin shell theory, we assume that: 1) The strains are small everywhere, but large rotations and deflections are admitted; and 2) the transverse shear deformation and transverse normal stress acting on the surface parallel to the middle surface may be neglected. In this theory, the bending strain is considered. A computer program [3,4] applying this nonlinear thin shell theory has been developed by Ford Research to compute the large deflection as well as the stress in the plastic range of a general thin shell structure. The curved triangular elements which can be proved to converge to the exact solution were adopted in this program; however, the shell surface must be C^1—slope

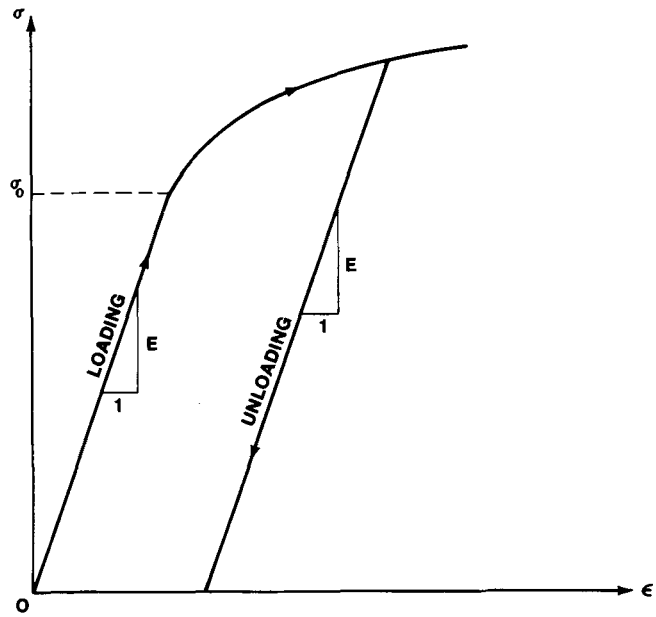

Fig. 4—Uniaxial stress-strain curve for a metal.

continuous everywhere. The elasto-plastic theory for the material properties was also used in this program; therefore, it can compute the permanent deformation and residual stress distribution when loads are completely released from a thin shell structure. The method used to solve the nonlinear problem is a step-by-step numerical integration method for each load increment. The special feature in this program is that an equilibrium check is made at each load step. If the unbalanced forces in the equilibrium check are unacceptable, an iteration which is similar to that of the Newton-Raphson method is used until the unbalanced forces are small.

This program can be applied without any modification to find the deformed shape of a blank during the binder-wrap stage in the sheet metal stamping process. The displacement boundary conditions are specified to the binder surface shape and the external loads are due to the weight of the blank and frictional forces acting on the blank in the blank holder contact area. To save computing time, we may neglect the deflection of the blank due to the plastic strain, so that we consider only the geometrical nonlinearity during the binder-wrap stage. We note that the radius R of the binder may be as small as 3 in. (7.62 cm) and that the maximum bending stress in the blank with thickness t = 0.030 in. (0.762 mm), according to the elastic cylindrical bending equation,

$$\sigma = \frac{E}{(1-\nu^2)} \cdot \frac{1}{R} \cdot \frac{t}{2} \qquad [3]$$

is greater than 100,000 psi (689.5 MPa) for steel with Young's modulus$E$ = 30 × 10^6 psi (207 GPa) and Poisson's ratio ν = 0.3. By observation, the plastic flow

due to this high stress is restricted to a very narrow region; therefore, it does not have a significant effect on the overall deflection, as shown by Lin *et al.*[5]

The specified displacements of the blank in the blank holder surface are large and have the order of magnitude of the blank length or width; thus, we must use the step-by-step increment of the displacements to reach the final specified values for a trial design of the binder surface shape. If we increased proportionally the resulting displacement at every boundary point until reaching the final specified values for the trial design, we would discover that there was a tremendous amount of membrane stresses involved during the computation process. This would cause difficulties in computation. As a matter of fact, this procedure is contrary to what happens in the real world during the binderwrap stage, because we observe that there is not much membrane stresses in the blank in the process to reach that stage. The membrane stresses increase to a tremendous amount and then decrease due to an artificially imposed increment of the displacement boundary condition —increasing proportionally at each boundary point. To do this naturally without excessive membrane stress increase or decrease in the computing process, we may increase the curvatures of the edges of a blank gradually from flat to the specified curvatures or decrease the radii from infinity (flat initially) to the specified amounts. A pre-process computer program, computing the displacement increments due to these radius changes, can be written without any difficulty and this program progressively prepares input data for the nonlinear shell program. Achieving the displacement boundary condition at edges in this way, we discovered that there were always bending stresses without excessive membrane stresses and accurate results were easy to obtain because of the weakness of the nonlinearity. After the boundary displacements specified by the trial design are reached, we can start to apply the external pressure due to the weight of the blank and the frictional forces acting on the edges of the blank. This procedure is justified for the nonlinear problem because we neglect the plastic flow which is loading path dependent. In the nonlinear elastic problem, the final result is independent of a loading path. This means we may load the structure in a way to suit computational convenience. As long as the same final loading condition is reached, the solution should not deviate from the desired one.

NUMERICAL EXAMPLES

The first example is a Thunderbird trunk deck lid made from a steel blank 48.625 in. (123.5 cm) × 70.840 in. (179.9 cm) × 0.033 in. (0.84 mm). The specified displacements at binder edges are shown in Fig. 5 where the coordinate system is the same as that in Fig. 1. Taking advantage of symmetry about the plane $y = 0$, we modelled half of the blank surface with 24 nodal points and 30 triangular elements, as shown in Fig. 6. In running the nonlinear shell program, we reduced the radii, shown in Fig. 5, gradually from infinity (flat) to the final values 199.510 in. (506.8 cm), 4.00 in. (10.2 cm), and 69.019 in. (175.3 cm), respectively, in the several steps tabulated in Table I. In each step, it took no more than four iterations to converge, *i.e.* the equilibrium conditions satisfied in the nonlinear shell program. After the displacements along edges specified by the trial design were reached, the weight of the blank equal to a uniformly distributed load of 0.0092 psi (0.063 kPa) was then imposed in the negative z-direction. Instead of applying the frictional forces acting on the blank edge, we pulled back the blank edge by 80 pct of the displacement in the y-direction computed previously. We tried to pull back the blank edge in the y-direction by various amounts (from 0 to 100 pct of the computed value). This pull back could change the deformation along two sides AO and BC in Fig. 1; however, it has negligible effect on the deformation of the profile P-P in Fig. 2. The deformed shape of the blank in the vicinity of that profile is the most important because the punch would contact that area first. The solution from pulling back by 80 pct seems to give the best agreement for the

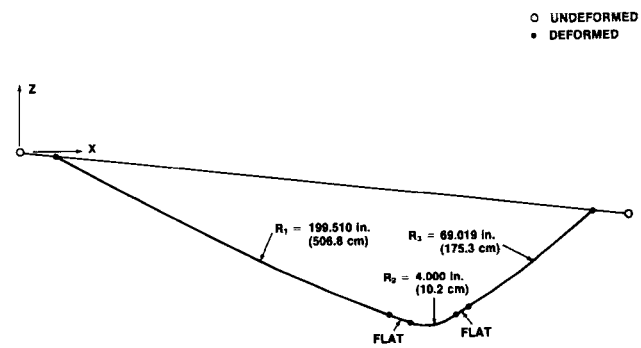

Fig. 5—Specified deformed edges of a blank in Example 1.

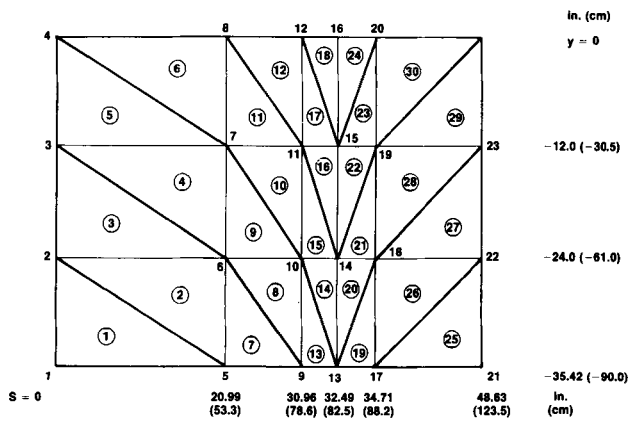

Fig. 6—Finite element model for the blank in Example 1.

deformation along these two sides with the measured values. In the last run, we froze the displacement boundary condition—no further movement of the binder edges in both x and z directions. The computer results for sections at y = 0, -12 in. (-30.5 cm), -24 in. (-61.0 cm), and -35.423 in. (-90.0 cm) in the final deformed state are shown in Figs. 7 and 8. At the section y = 0, we actually measured the deformation of the trial blank in the plaster shop. Excellent agreement between the computed and measured results is shown in Fig. 7.

The second example is a Fairmont/Zephyr trunk deck lid made from a steel blank 53.318 in. (135.4 cm) × 69.00 in. (175.3 cm) × 0.033 in. (0.84 mm). The specified displacements at binder edges are shown in Fig. 9 where the coordinate system is also the same as that in Fig. 1. Taking advantage of symmetry about the plane y = 0, we modelled half of the blank surface with 33 nodal points and 43 triangular elements, as shown in Fig. 10. In running the nonlinear shell program, we reduced the radii, shown in Fig. 9, gradually from infinity to the final values 28.985 in. (73.62 cm), 3000 in. (7.62 cm), 4.100 in. (10.41 cm), and 10 in. (25.40 cm), respectively, in the several steps tabulated in Table II. We used the same strategy to treat the weight of the blank and the frictional forces as that described in Example 1. The computer result for the center section at y = 0 in the final deformed state is shown in Fig. 11. The actually measured values from the trial blank in the plaster shop are also shown in the same figure. Excellent agreement between the computed and measured results was also obtained in this example.

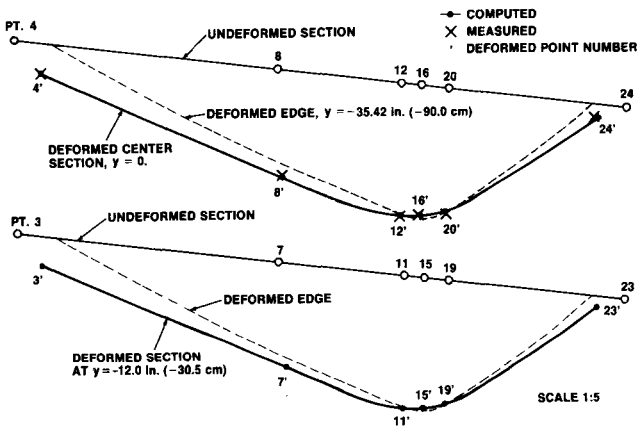

Fig. 7—Deformed shape at sections y = 0 and -12 in. (-30.5 cm) for Example 1.

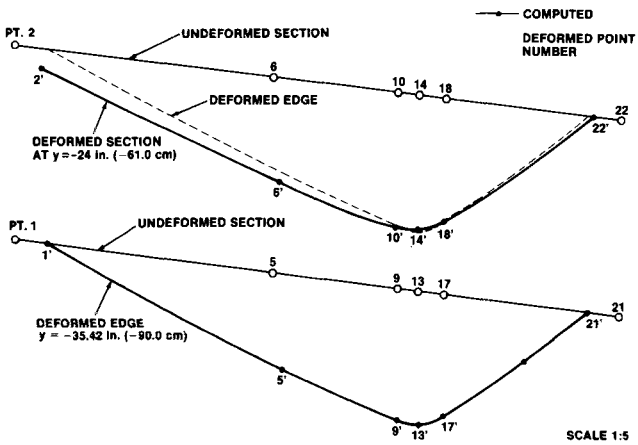

Fig. 8—Deformed shape at sections y = -24 in. (-61.0 cm) and -35.42 in. (-90.0 cm) for Example 1.

Table I. Reduction of Radii for Example 1

No.	R_1 in. (cm)	R_2 in. (cm)	R_3 in. (cm)
1	∞	500 (1270)	∞
2	∞	300 (762)	∞
3	∞	200 (508)	∞
4	∞	100 (254)	∞
5	∞	50 (127)	∞
6	∞	25 (63.5)	∞
7	∞	15 (38.1)	∞
8	500 (1270)	10 (25.4)	500 (1270)
9	300 (762)	8 (20.3)	300 (762)
10	199.510 (506.8)	6 (15.2)	100 (254)
11	199.510 (506.8)	5 (12.7)	69.019 (175.3)
12	199.510 (506.8)	4 (10.2)	69.019 (175.3)

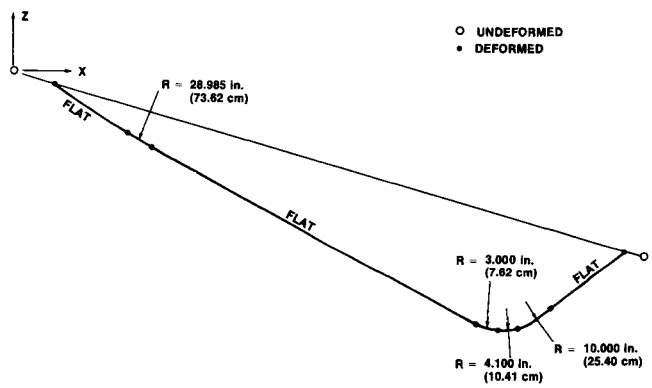

Fig. 9—Specified deformed edges of a blank in Example 2.

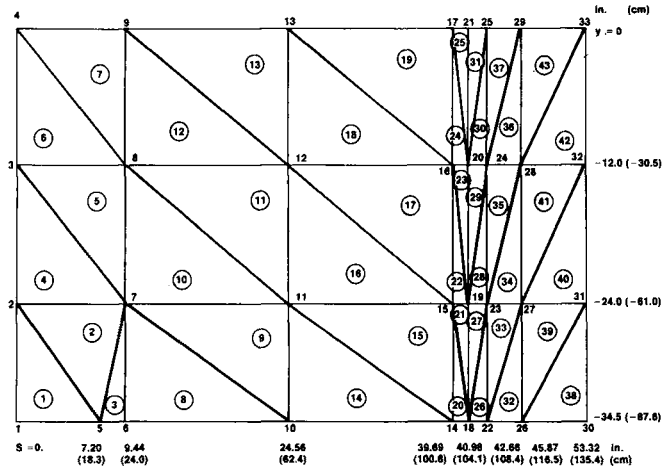

Fig. 10—Finite element model for blank in Example 2.

Table II. Reduction of Radii for Example 2

No.	R_1 in. (cm)	R_2 in. (cm)	R_3 in. (cm)	R_4 in. (cm)
1	∞	500 (1270)	500 (1270)	500 (1270)
2	∞	300 (762)	300 (762)	300 (762)
3	∞	100 (254)	100 (254)	100 (254)
4	∞	70 (177.8)	70 (177.8)	70 (177.8)
5	∞	50 (127)	50 (127)	50 (127)
6	∞	35 (88.9)	35 (88.9)	35 (88.9)
7	∞	20 (50.8)	20 (50.8)	20 (50.8)
8	∞	13 (33.0)	13 (33.0)	33 (33.0)
9	500 (1270)	10 (25.4)	10 (25.4)	10 (25.4)
10	300 (762)	8 (20.3)	8 (20.3)	10 (25.4)
11	200 (508)	6 (15.2)	6 (15.2)	10 (25.4)
12	100 (254)	5 (12.7)	5 (12.7)	10 (25.4)
13	70 (177.8)	4 (10.2)	4.1 (10.4)	10 (25.4)
14	40 (101.6)	3.5 (8.9)	4.1 (10.4)	10 (25.4)
15	28.985 (73.6)	3.0 (7.6)	4.1 (10.4)	10 (25.4)

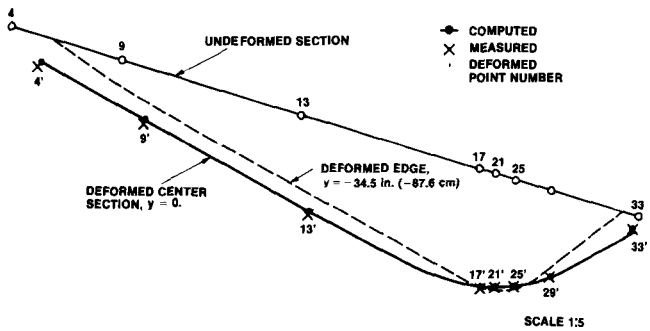

Fig. 11—Deformed shape at the center section $y = 0$ for Example 2.

CONCLUSION

We have described a method to predict accurately the deformed shape of a draw blank during the binder-wrap stage in the sheet metal stamping process by the application of a nonlinear shell computer program. For the two numerical examples of body panels with center line symmetry described in this report, the boundary conditions were displacements specified at the parallel punch opening sections; therefore, the two sides near the center section could open up—double butterfly, so called. We have applied this method to predict the case of a symmetrical body panel where the displacements along a third side were also specified as a straight through and only one side was free and could open up, so called single butterfly. Accurate results for the blank with displacements specified along three sides were also obtained from the computer program. For a nonsymmetric body panel, the described method can still be applied; however, we must model the whole blank and the computing time increased by a factor of two is expected. As a matter of fact, any well posed nonlinear boundary value problem, with either force or displacement properly specified at any point, can be solved accurately by means of this nonlinear shell computer program.

The only restriction of this program is that strains in the blank must be small, say, less than 5 pct in the final deformed state. Strains in a typical deformed blank during the binder-wrap stage are well below that amount. Even after the punch initially contacts the blank, strains in the blank will only approach the 5 pct level; therefore, we can utilize this program to predict stresses and deformation into that stage, as well.

However, as the punch moves further, strain in the blank will exceed 5 pct and then large strain analysis must be invoked in order to predict correct stresses and deformation. The nonlinear shell theory for large strains is still under development. Therefore, we hope in the near future to develop a similar computer program to predict stresses and deformation for all stages in the sheet metal stamping process.

As to the computing time for the prediction discussed in this report, it depends upon the number of elements used in the model and the size of the computer. For example, if a CDC Cyber 175/176 computer is used and the binder surface is not so complicated that one hundred shell elements are fine enough to model the blank, the computing time will be no more than 30 minutes.

APPENDIX

The Finite Element Method

The basic concept is that the finite element method treats a loaded structure as being built up of numerous tiny connected substructures or elements. The elements can be of various shapes, but we shall discuss the simplest shape, *i.e.* triangle. Points on corners where the elements are connected to one another are called nodes and are indicated by dots in Fig. 12. In the most popular displacement method, a set of functions —known as the shape or interpolation functions—is chosen to define uniquely the state of displacement within each element in terms of its nodal displacements. The state of strain in an element can be expressed in terms of the nodal displacements by means of the strain -displacement relationship:

$$\underset{\sim}{\epsilon} = \underset{\approx}{B}\underset{\sim}{\delta}_e \qquad [A1]$$

in which $\underset{\sim}{\epsilon}$ is a strain vector, $\underset{\sim}{\delta}_e$ is an element nodal displacement vector, and $\underset{\approx}{B}$ is a matrix uniquely determined by assigned element displacement function. In a general multi-axial stress problem, the strain $\underset{\sim}{\epsilon}$ at a point has

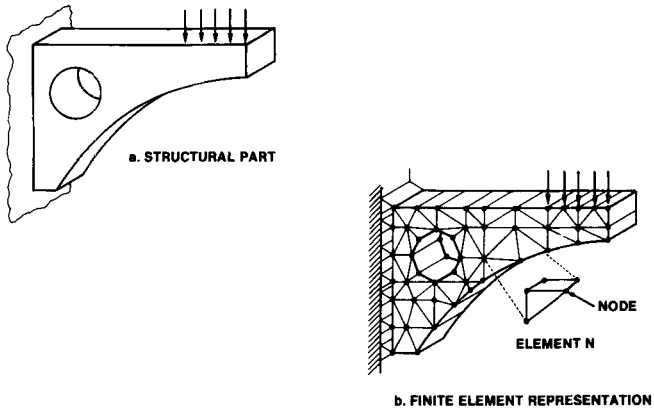

Fig. 12—Translation of a load-bearing part to a finite element representation.

more than one component so that it is expressed by a vector. There is more than one displacement component for each node and there is more than one node for each element; therefore, the nodal displacement for an element has more than one component and it is also represented by a vector. From the mechanical property of a material, we can relate the stress vector $\underset{\sim}{\sigma}$ in an element to the strain vector $\underset{\sim}{\epsilon}$, as follows:

$$\underset{\sim}{\sigma} = \underset{\approx}{D}\underset{\sim}{\epsilon} \qquad [A2]$$

In a linear-elastic uniaxial stress state, the material matrix $\underset{\approx}{D}$ reduces to Young's modulus E and Eq. [A2] is the well known Hooke's Law. For a linear isotropic elastic material, Eq. [A2] is the generalized Hooke's Law. In this case, the matrix $\underset{\approx}{D}$ only contains two independent material parameters—Young's modulus E and Poisson's ratio ν. Substituting $\underset{\sim}{\epsilon}$ from Eq. [A1] into Eq. [A2] gives

$$\underset{\sim}{\sigma} = \underset{\approx}{D}\underset{\approx}{B}\underset{\sim}{\delta}_e \qquad [A3]$$

In the finite element method, we establish the force equilibrium only at a set of discrete points, the nodal points: therefore, we want to compute equivalent nodal forces. Applying the equilibrium condition or the principle of virtual work, we obtain

$$\underset{\sim}{f} = \int_v \underset{\approx}{B}^T \underset{\sim}{\sigma} dv \qquad [A4]$$

in which $\underset{\sim}{f}$ is the nodal force vector of an element and its components are one to one corresponding to those of the nodal displacement vector $\underset{\sim}{\delta}_e$, the superscript T denotes the transpose of a matrix (interchange of rows and columns), and $\int_v$ is the integration over the element volume. For a special case of a constant strain triangle in a plane stress problem, Eq. [A4] reduces to

$$\underset{\sim}{f} = \underset{\approx}{B}^T \underset{\sim}{\sigma} t\Delta \qquad [A5]$$

in which t is the uniform thickness and δ the area of a triangle. Combination of Eqs. [A3] and [A4] gives for each element

$$\underset{\approx}{k}\underset{\sim}{\delta}_e = \underset{\sim}{f} \qquad [A6]$$

in which the element stiffness matrix

$$\underset{\approx}{k} = \int_v \underset{\approx}{B}^T \underset{\approx}{D}\underset{\approx}{B} dv \qquad [A7]$$

The meaning of Eq. [A6] can be illustrated by an elastic spring in Fig. 13. The force f_i is related to the displacement u_i by the equation $ku_i = f_i$, where k is the spring stiffness coefficient, defined as the force required at a point to produce a unit displacement at that point. After we establish the stiffness equation as that in Eq. [A7] for each element, we assemble them into a global one.

$$\underset{\approx}{K}\underset{\sim}{\delta} = \underset{\sim}{F} \qquad [A8]$$

in which $\underset{\sim}{\delta}$ is the global nodal displacement vector containing all nodes in a structure, $\underset{\sim}{F}$ is the nodal force vector including the equivalent forces due to distributed load, and K is the global stiffness matrix.

Before we are able to solve $\underset{\sim}{\delta}$ in Eq. [A8], we must impose some constraints—supporting or loading conditions. If only loads are prescribed, Eq. [A8] can be solved for $\underset{\sim}{\delta}$ in a straightforward manner. However, special techniques will be required to obtain solutions for unknown components in both $\underset{\sim}{\delta}$ and $\underset{\sim}{F}$ if there are displacement constraints. One of the techniques requires, prior to the solution, the rearrangement of Eq. [A8] in such a way that the known components in $\underset{\sim}{\delta}$ be separated from the unknown components. This involves considerable effort; therefore, it is not recommended. There are two known techniques[1,6] to modify $\underset{\approx}{K}$ and $\underset{\sim}{F}$ in Eq. [A8] without rearranging Eq. [A8] for solving $\underset{\sim}{\delta}$. The classic Gauss elimination method is the most popular one to solve this set of linear simultaneous algebraic equations. Once the nodal displacement vector $\underset{\sim}{\delta}$ is known, we can then compute the strain and stress from Eqs. [A1] and [A2] for every element in the structure. Thus, the problem is solved.

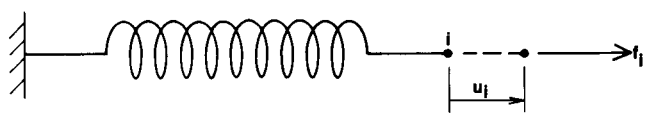

Fig. 13—Elastic spring illustrating the concept of a stiffness coefficient.

ACKNOWLEDGMENT

The author wishes to thank R. C. Petrof and K. S. Yeung for reading the manuscript and J. Heetderks of MSD and W. G. Brazier of BEPE for valuable comments on this work.

REFERENCES

1. W. C. Paulsen: *Mach. Des.*, 1971, vol. 43, no. 23, pp. 46–52, no. 25, pp. 146–50, and no. 26, pp. 90–94.
2. A. Mendelson: *Plasticity: Theory and Application*, p. 100, McMillan, New York, 1968.
3. S. C. Tang: *Computers and Structure*, 1976, vol. 6, pp. 297–303.
4. S. C. Tang: *Proceedings of the 2nd International Conference on Vehicle Structural Mechanics*, SAE, 1977, pp. 1–8.
5. T. H. Lin: *et al. J. Appl. Mech.*, 1972, vol. 39, pp. 978–81.
6. O. C. Zienkiewicz: *The Finite Element Method in Engineering Sciences*, p. 457, McGraw-Hill, London, 1971.